

PHANTOM BLADE MODEL – ADVANCED METHODOLOGY FOR ACTUATOR DISK MODELING

T. Dos Reis Marioni, G. Legras

Airbus Helicopters S.A.S., Marseille Provence International Airport, F-13725 Marignane cedex, France

S. Link, M. Embacher

Airbus Helicopters Germany GmbH, Industriestraße 4, D-86609 Donauwörth, Germany

Abstract

A good prediction of the unsteady behavior of the aerodynamic interactions between rotating and fixed parts is of great importance in the design of a helicopter, in particular for rear parts conception. In the present work, an unsteady actuator disk-like approach named Phantom Blade Model (PBM) is presented and results obtained are confronted to other numerical approaches and test data. This method allows (1) improved modeling of the rotor downwash and of the aerodynamic interactions compared to the classic, steady, actuator disk and (2) reduced pre-processing and computational times compared to high-fidelity CFD models with meshed blades. First, two academic cases for which experimental data is available, namely an isolated two-bladed rotor in hover and a ROBIN fuselage equipped with a four-bladed rotor in level flight, are used as validation cases for the PBM. Good agreement is observed with both tests and meshed-blades simulations, with reduced simulation time – 48% and 63% less CPU hours, respectively. Then, the PBM is applied to the Bluecopter® in forward flight, in which PBM is used for both main rotor and Fenestron®. Comparison between high-fidelity CFD/CSM simulations of a full helicopter, flight tests and unsteady actuator disk applied to a flying aircraft as presented here is new. Results with PBM of unsteady loads and pressure at the horizontal stabilizer are considerably close to the complete helicopter CFD/CSM simulations. Both numerical methods fairly capture the amplitudes, but slightly overestimate the average pressure compared to test data.

1. INTRODUCTION

Correctly predicting the unsteady aerodynamic interactions between rotating and fixed parts is essential in the design process of a helicopter. In particular, vertical and horizontal stabilizers on a conventional helicopter are most often exposed to the rotor wake and tip vortices, as are wings downstream of propellers on hybrid helicopter configurations. Failing to properly assess the dynamic loads on these parts early in the development can cause costly and time-consuming redesign work later during flight tests.

The natural approach for the simulation of the interactions is a complete helicopter CFD numerical model, eventually coupled with a flight mechanics code for trim and blade elasticity.^{[1][2]} This method, however, can be quite expensive in terms of model preparation and computational time. Therefore, in early helicopter design process a lower fidelity tool with short lead-time may be convenient.

In the present work, an unsteady actuator disk-like approach named *Phantom Blade Model* (PBM) was presented and implemented using the ONERA CFD code elsA^[3] and results obtained were confronted to higher fidelity numerical approaches and test data. A

first prototype of the PBM methodology was already implemented in Airbus Helicopters using CFD code FLUENT, but no thorough validation was done.

The main interest of such a methodology is the possibility of modeling unsteady phenomena related to the rotating blades without having to mesh or compute them. Consequently, preparation and computational cost of the PBM is significantly reduced when compared to simulation with meshed blades. This is particularly convenient for the aforementioned applications where rotor downwash and fixed parts dynamic interactions are of interest.

Although similar methodologies with different tools based either on volume or surface source terms for blades representation can be found^{[4][5]}, a comparison between a full helicopter CFD model, flight tests and unsteady actuator disk applied to a flying aircraft as presented here is new.

2. IMPLEMENTATION STRATEGY

In elsA, an actuator disk modeling of the rotor wake is already available. This implementation is based on surface source terms added to the convective fluxes

of Navier-Stokes' equations which result in an energy and momentum increase throughout the whole disk discontinuity surface^[6].

In order to improve the representativeness of the actuator disk for time-dependent aerodynamic interactions, an unsteady version was implemented in elsA, the Phantom Blade Model (PBM). As for the steady actuator disk, rotor downwash is simulated by energy and momentum source terms, but in the PBM approach, blades planform and position are represented through the activation of *volume* source terms – also known as body-force^[7] - in specific mesh cells at each time step.

Although rotor loads are usually computed using the comprehensive helicopter flight mechanics code HOST^[8] (Figure 1) any method to obtain the loads distribution is compatible with the PBM approach, including extraction from CFD rotor computations, for example.

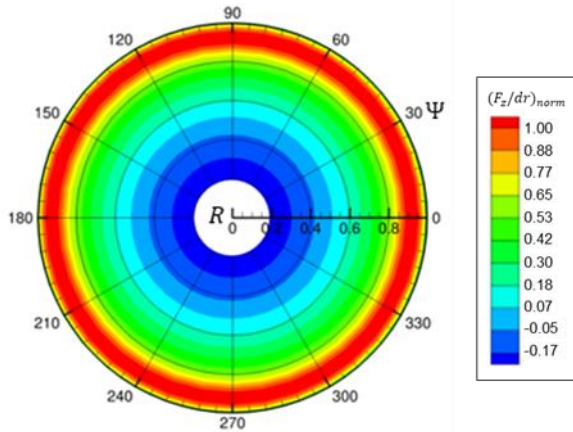


Figure 1: Example of HOST loads mapping used as an input for actuator disk modeling in elsA. Vertical force normalized by the maximum value. Two-bladed rotor in hover.

This implementation makes use of elsA's existing interoperability capability, which allows accessing solver in-memory data through an external Python script.^[9]

2.1. PBM Mesh

From a few parameters such as minimum and maximum rotor radii and discretisation number of points, the actuator disk structured mesh is automatically generated. A cylindrical topology – i.e. H-mesh with both ends connected in one direction – is used to model the actuator disk as only the mesh central layer in the *z* direction is filled. This choice is convenient for the rotor representation since quantities are usually described in a cylindrical frame (*R*, Ψ , *z*) (Figure 2).

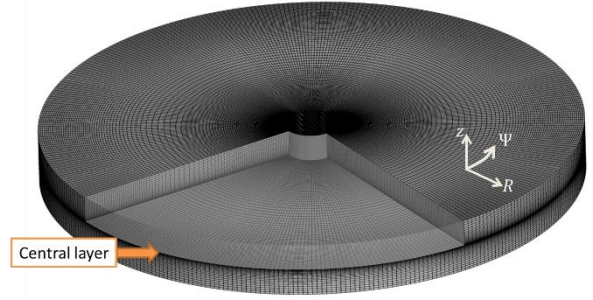


Figure 2: Example of an actuator disk structured H-topology mesh. The central layer where the source terms will be imposed is indicated.

Finally, blade coning and flapping angles can be accounted for through mesh deformation in the direction normal to the disk. The PBM implementation is independent of the mesh shape since the central layer nodes indexes are not modified with the deformation.

2.2. Blade representation

As shown in Figure 3, at a given time *t*, the azimuthal position of each blade defines a local frame (*x'*, *y'*). Then, for each blade element defined by the user (radius, chord, aerodynamic center), four points are placed corresponding to the leading and the trailing edges at *R_i* and *R_{i+1}* stations. Finally, four lines bounding the blade element are used to tag all cells whose center is within the identified region. Blade thickness is not modeled, as only the central mesh layer is filled with source terms.

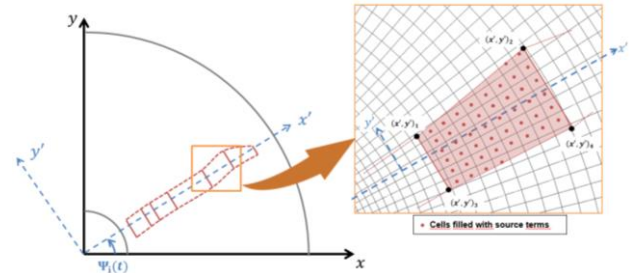


Figure 3: Principle of blade positioning and shape representation in PBM.

2.3. Source terms

Radial and azimuthal interpolations of rotor loads mapping into the CFD mesh are performed. In addition, as to limit the source terms discontinuity at the leading and trailing edges due to the mesh discretisation, the loads are distributed over the chord using the linear function below as illustrated in Figure 4:

$$(1) \quad f_i(\bar{x}) = \begin{cases} 2F_i \frac{\bar{x}}{0.25}, & \text{if } 0 \leq \bar{x} \leq 0.25 \\ 2F_i \frac{(1-\bar{x})}{0.75}, & \text{if } 0.25 < \bar{x} \leq 1 \end{cases}$$

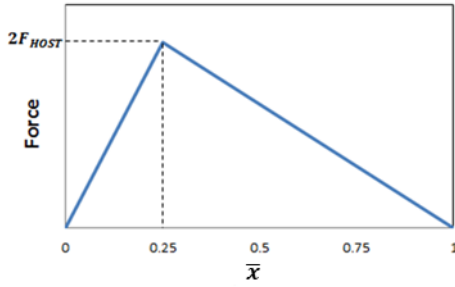


Figure 4: Chordwise loads distribution. Force is set to zero at $\bar{x} = 0$ and $\bar{x} = 1$ to limit the discontinuities at the leading and trailing edges.

The cells in the central mesh layer within the blade planform located at azimuth $\Psi(t)$ are then filled with source terms as follows:

- (2) $S_i = \frac{F_i}{Vol}$, with $i = x, y, z$ for momentum source terms, where F_i and Vol represent aerodynamic forces and the cell volume, respectively.
- (3) $S_E = \sum_i \frac{F_i v_i}{Vol}$ with $i = x, y, z$ for energy source term, where v_i represents the local velocities.
- (4) $S = \mathbf{0}$ for all turbulent variables.

In all other cells, source terms are set to zero (Figure 5).

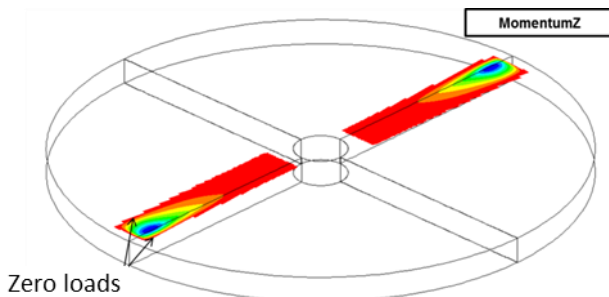


Figure 5: Resulting Z momentum applied using PBM.

The main limitation of the PBM approach is evidently the fact that it does not predict the rotor loads since they are imposed.

2.4. Numerical parameters

The numerical simulations performed in the frame of the present work were all conducted using the ONERA's CFD code elsA, which solves the Unsteady Reynolds-Averaged Navier-Stokes (URANS) equations in multi-block structured meshes. Flow is assumed fully turbulent and the chosen model is the two-equation $k - \omega$ with Shear Stress Transport (SST) with Menter's correction.^{[10][11]} Fluxes are computed using the second-order central JST

scheme with artificial dissipation^[12]. Chimera technique was employed in the assembly of the near-body and background grids with second-order interpolation for the data exchange between overset grids.^{[13][14]} Unsteady simulations were performed using a dual-time step (DTS) approach^[15] with an efficient implicit time integration scheme based on the backward Euler scheme.

3. RESULTS

Three applications were selected in order to evaluate the implemented PBM with increasing level of complexity and representativeness of a real helicopter. First of all, tests with an isolated two-bladed rotor in hover performed by Caradonna & Tung^[16] were used to assess the ability of the PBM to predict the rotor downwash characteristics. Secondly, wind tunnel tests of the ROBIN equipped with a four-bladed rotor conducted by Freeman & Mineck^[17] provide a rich database of dynamic interactions through unsteady pressure measurements on the fuselage. Finally, the PBM was applied to the Bluecopter® in forward flight (130kt) and results were confronted both to complete H/C fluid-structure coupled simulations^[18] and flight test data.

3.1. Two-bladed isolated rotor

Experimental investigations of an isolated two-bladed rotor in hover were conducted by Caradonna & Tung^[16] in which blade tip trajectories characterizing the rotor downwash were measured. The rotor had a radius of $1.143m$ and the blades were composed of NACA0012 airfoils with constant chord of $0.1905m$, constant thickness and no twist (Figure 6). Several rotor rotating speeds and blade pitch angles were tested, but the case chosen for the present work is $\theta = 8^\circ$ and $\Omega = 1750rpm$, corresponding to a blade tip speed of $V_{tip} = 209.5m/s$ or Mach number $Ma = 0.62$.

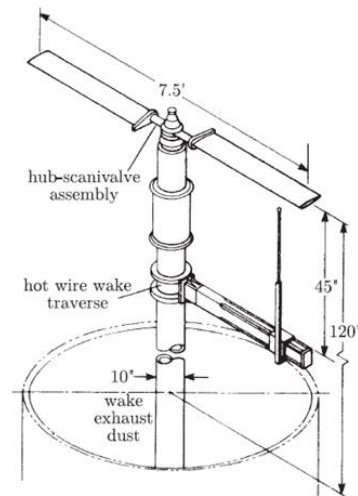


Figure 6 : Experimental setup of an isolated two-blade rotor (From Caradonna & Tung^[16]).

Two numerical models were set up, the first one with meshed blades and the second one with PBM. In both cases a simplified fixed mast consisting of a 0.1905m diameter and 2-rotor-radii length cylinder was included. Identical Cartesian background grids, refined to around 5% of the blade chord in the proximity of the rotor, were used in both the meshed-blades and PBM models (Figure 7). The total mesh assembly resulted in 76.1M and 64.5M elements, respectively.

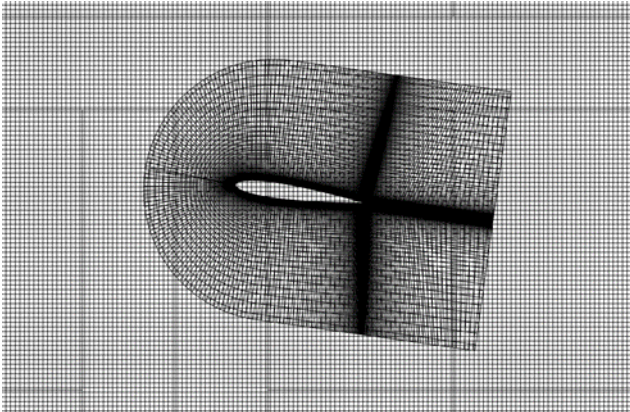


Figure 7: Section view of blade and background meshes. Background grid refinement level near the rotor correspond to 5% of the blade chord.

The convergence strategy consisted in 10 rotor revolutions at a time-step equivalent to $\Delta\Psi = 10^\circ$ and 20 sub-iterations, then 2 revolutions at $\Delta\Psi = 1^\circ$ and 10 sub-iterations. Whereas the meshed-blades simulation requires repositioning the blocks and recomputing masking and interpolations for Chimera at each time step, in the PBM approach the rotor disk mesh is fixed so the masking and interpolations are frozen. Along with the slightly smaller grid count, this contributes to reducing the simulation CPU time by 48% when using PBM.

Regarding the rotor loads for the PBM, two different sources were used for comparison. First, rotor loads were obtained through an isolated rotor trim in HOST using METAR's induced velocity model.^[19] Secondly, aerodynamic loads on the blades were directly extracted from the meshed-blades CFD simulation. Figure 8 compares the resulting lift distribution along the span, which is independent of the azimuth of the blade for an isolated rotor in hover. One can see that in the loads extracted from the CFD simulations lift is generated from the very blade root which will create a shear flow in the zone and that the maximum lift is concentrated near the blade tip. The HOST radial lift distribution, on the other hand, is smoother near the blade root but with a larger region with high lift. Despite the differences in these distributions, the total blade lift obtained through integration of the curves is quite close (less than 5% delta).

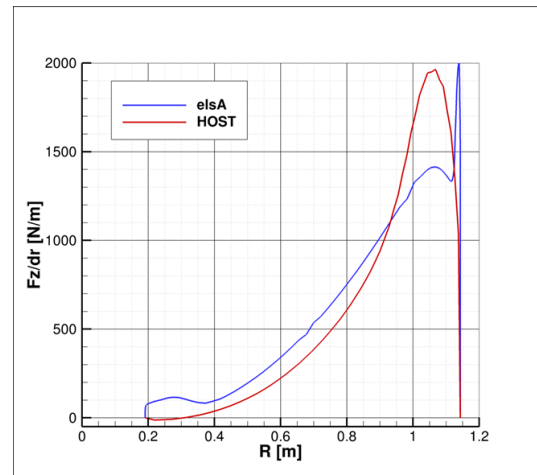


Figure 8 : Lift loads distribution along the blade span. Comparison between loads from HOST and extracted from a CFD computation.

Figure 9 compares Z-velocity contours on a slice passing through the rotor axis between meshed-blades, PBM with HOST loads and PBM with CFD loads simulations. Z-velocity field is globally comparable between all three methods. Blade tip vortices are generated and the rotor downwash contraction is observed. However, the PBM with HOST loads simulation yields stronger blade tip vortices and almost no recirculation near the blade root, compared to meshed-blades. This is consistent with the loads distribution of Figure 8. In the third case, with loads from CFD, the PBM performs better at the blade root where a positive Z-velocity region comparable to meshed-blades results appears, but the blade tip vortices are weaker. One possible reason is the mesh refinement of the disk, as in the direction normal to the disk only 22 layers are present against 97 in the blade mesh. Moreover, the azimuthal discretization was of 360 points which corresponds to a grid size of more than 10% of the blade chord near Chimera interpolation layers. As a consequence, vortices convection and Chimera interpolations may have suffered from insufficient grid resolution. Rotor wake of PBM with HOST loads is slightly asymmetric due to flow instabilities near the lower farfield boundary condition. However, post-processing of blade tip trajectories at two different time steps showed little impact from the instable flow, at least up to 450° of vortex age.

Blade tip vortex trajectory was determined by the local maxima of X and Y-vorticity on the YZ and XZ planes, respectively. An age is then associated to the vortex corresponding to the blade azimuthal position where it was generated. Figure 10 compares results from all three numerical approaches to experimental data obtained by Caradonna & Tung.^[16] Axial convection and radial contraction are slightly overestimated by CFD simulations – both meshed-

blades and PBM – but they are able to capture the interaction between vortex and next blade passage which accelerates the axial convection at 180°. It is clear that the PBM with more representative loads, in this case extracted from a CFD simulation, results in a better blade tip trajectory prediction. As it would be too costly to perform meshed-blades CFD simulations to generate PBM inputs, a potential improvement of the method would consist in coupling PBM with HOST to iteratively correct the induced velocity model and obtain more representative loads distributions.

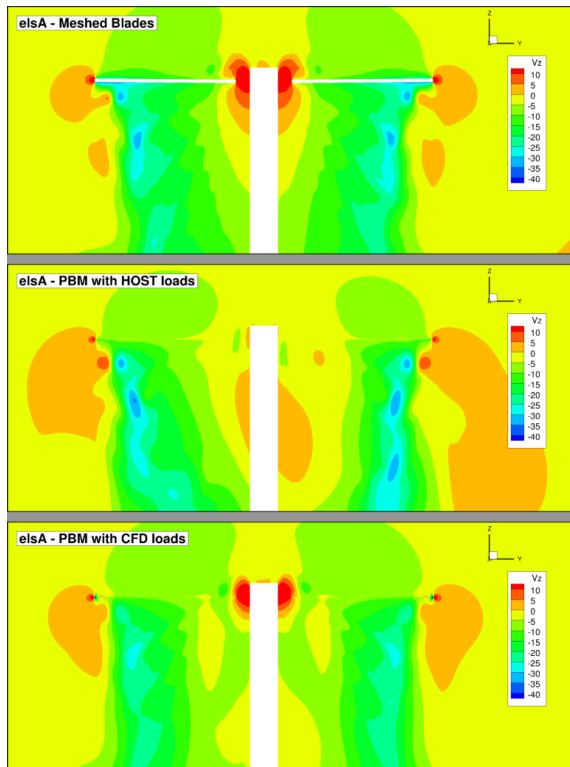


Figure 9 : Z-velocity contours on slice passign through the rotor axis. Meshed-blades CFD (top), PBM with HOST loads (middle) and PBM with CFD loads (bottom).

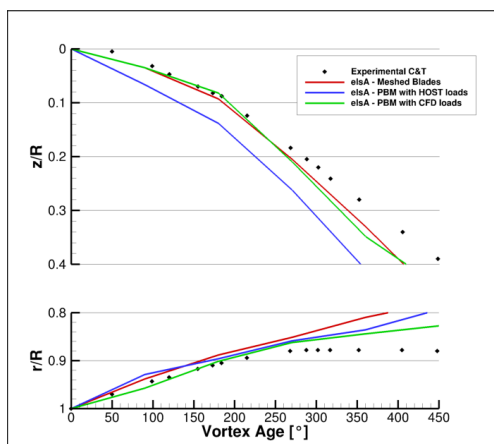


Figure 10 : Blade tip vortices trajectories. Axial convection (top) and radial contraction (bottom). Comparison between meshed-blades CFD, PBM (HOST and CFD loads) and experimental data (dots) from Caradonna & Tung.^[16]

3.2. Rotor-fuselage interaction

The second test case used in the PBM validation is a ROBIN fuselage equipped with a four-bladed rotor, tested in a wind tunnel by Freeman & Mineck.^[17] The fuselage is 1m-long. Blade airfoil is a NACA0012, with 0.86m radius and 0.1905m constant chord. The blade is untwisted and unswept. Mast is positioned with an angle of -3° (Figure 11).



Figure 11: View of the experimental setup of the ROBIN fuselage equipped with a four-bladed rotor.^[17]

Several rotor advance ratios and thrust coefficients were tested. The selected case to validate the representativeness of rotor-fuselage interactions with the PBM corresponds to $\mu = 0.15$ and $C_T = 0.0064$. Rotor rotating speed is $\Omega = 2000rpm$, corresponding to a blade tip speed of $V_{tip} = 108.14m/s$.

As for the previous test case, two numerical models were set up, one with meshed-blades and another with an actuator disk mesh for the PBM. The disk mesh was not deformed to account for coning and flapping angles, as this feature was not available at the time this application was studied. The Cartesian background grid is exactly the same in both models and is refined near the rotor and fuselage upper parts to around 5% of the blade chord (Figure 12). Regarding the Chimera assembly, blades, fuselage and disk mesh are masked in and exchange information with the background grid. Blades are repositioned by elsA according to the blade pitch, flap and lead-lag angles, so masking and interpolation coefficients have to be recomputed at each time step. With PBM, these operations are performed once at the beginning of the simulation since all the blocks are fixed throughout the computation. Meshed-blades grid has 82.1M elements whereas PBM mesh has 61.1M, about 25% less.

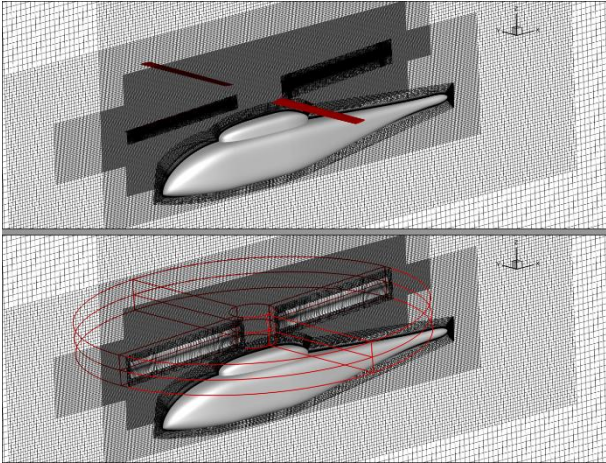


Figure 12: View of the mesh assemblies with blades (top) and with actuator disk (bottom).

Rotor harmonics used to position the blades were computed using HOST. The four-bladed rotor HOST model was trimmed using FISUW induced velocity model^[20] to a given rotor thrust and to zero flapping angles, resulting in the controls shown in Table 1.

Table 1: Blade pitch controls obtained through HOST trim simulation

HOST - FISUW ^[20]		
θ_0	θ_c	θ_s
6.9°	1.94°	-1.27°

The convergence strategy was similar to the previous case, with 10 rotor revolutions at a time-step equivalent to $\Delta\Psi = 10^\circ$ and 20 sub-iterations, then 2 revolutions at $\Delta\Psi = 1^\circ$ and 10 sub-iterations. Moreover, two additional rotor revolutions at $\Delta\Psi = 1^\circ$ to extract the surface solution at each time step were run. Time per iteration was divided by two with the PBM compared to meshed-blades simulation and 63% less CPU hours were necessary. The reduced computational time is due both to the reduced number of points and the frozen Chimera interpolations of the PBM model.

First, a comparison between the two numerical methods is made through flow visualization. In Figure 13, Z-velocity contours are represented on a $Y = 0m$ slice, on which surface streamlines are also shown. In addition, Q -criterion^[21] iso-surfaces at Q -criterion = $2000\text{rad}^2/\text{s}^2$ highlight the unsteady structures generated by the rotating blades. PBM is able to capture the unsteady features of the rotor wake, but a smaller deflection is observed when compared to meshed-blades results. This is also observed in the local angle of attack contours on a cross-section at $X = 1.47m$ (at $0.7R$ of rear blade) shown in Figure 14. At the rotor level, the local angle of attack is comparable between both methods, but nearer to the body angles are 5° to 10° smaller with the PBM. Similarly to the isolated two-bladed rotor, the disk grid resolution is assumed too coarse compared to the blade mesh, increasing the dissipation of the rotor wake.

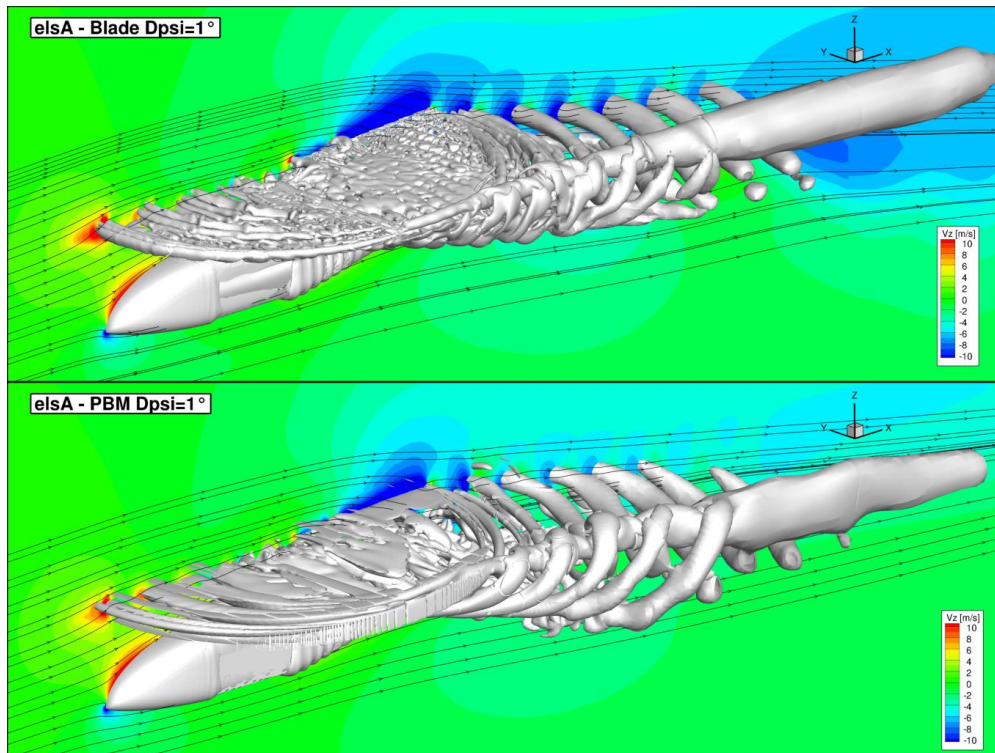


Figure 13: Flow visualization with Q -criterion iso-surfaces at $2000\text{rad}^2/\text{s}^2$, streamlines and Z-velocity contours on a slice $Y = 0m$. Meshed-blades (top) and PBM CFD simulations (bottom).

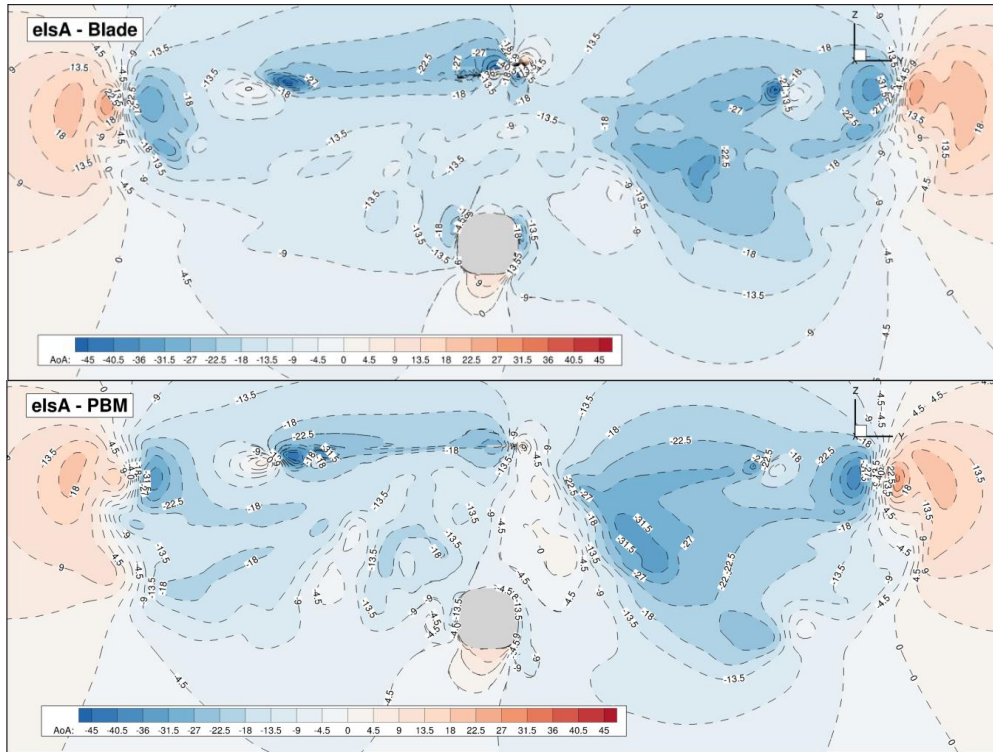


Figure 14: Flow visualization of local angle of attack on slice $X = 1.47m$. Meshed-blades (top) and PBM CFD simulations (bottom).

Then, results from numerical simulations are confronted to test data measured by Mineck & Freeman.^[17] Unsteady pressure measurements located along the upper fuselage centerline are expressed as pressure coefficient through normalization by the blade tip velocity V_{tip} , i.e.:

$$(5) \quad 100x C_p = 100 \frac{p - p_0}{\rho_{inf} V_{tip}^2}$$

Where ρ_{inf} and $p_0 = 101325Pa$ represent the upstream density and static pressure, respectively. Additionally, as pointed out by Kenyon & Brown, test data was corrected by a phase shift of 252° to account for issues in the data acquisition system.^[22] Figure 15 presents C_p evolution on 11 positions on the surface of the fuselage over one rotor revolution from numerical simulations with PBM and meshed-blades and experimental data.

Overall, PBM is in phase with meshed-blades model and the amplitudes are comparable, but it slightly underestimates the average pressure. In the front part of the fuselage, both simulations result in higher amplitudes, higher average pressure and a phase shift of around 20° compared to test data (test curves include phase shift correction mentioned above), the only exception being probe D9 where the pressure

dynamics and levels are close to measurements. The fact that the blade pitch controls are obtained through a trimmed HOST simulation is presumably at the origin of the observed differences. Indeed, a coupling between CFD and HOST to account for fuselage effects should be performed to obtain more accurate controls.

Probes D17 and D18 on the front chimney see little dynamics since they are close to the blade root, which is also observed in the numerical simulations. In the rear part of the chimney (D26), however, both PBM and meshed-blades CFD fail to capture the under pressure measured. Instead, an overpressure shifted by about 45° is observed. It must be pointed out that this probe is in the direct wake of the rotor head and the mast which were present in the wind tunnel tests, but not modeled in the CFD computations due to the lack of information about their geometry.

In the rear fuselage, the best agreement between numerical methods and experimental data is observed, despite the fact that the 20° -phase shift subsists. Similar phase shift was already observed in other studies in the literature, but no insight about its source was found.^[23]

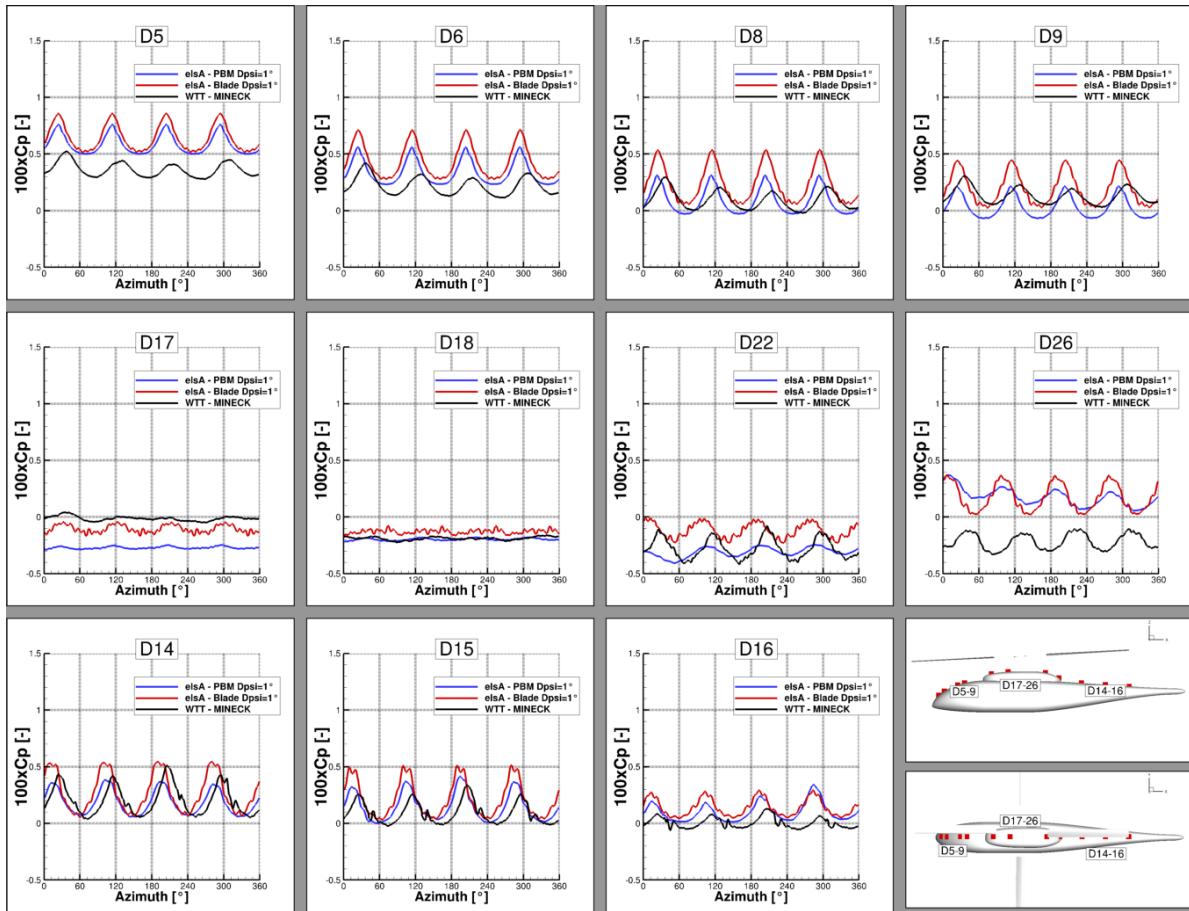


Figure 15: C_p evolution over one rotor revolution on the upper fuselage centerline. Comparison between meshed-blades and PBM numerical methods and experimental data from Freeman & Mineck.^[17]

3.3. Bluecopter®

The Bluecopter®, shown in Figure 16, is a helicopter demonstrator equipped with a 5-bladed rotor and a T-Tail, i.e. a horizontal stabilizer on the tip of the vertical fin.^[24] Although convenient to avoid low-speed rotor/T-Tail interactions causing high mast loads, this configuration has the drawback of having the rear parts constantly under the influence of the rotor unsteady wake at moderate and high-speed forward flight, generating significant dynamic loads at the rear parts. The correct prediction of this dynamic behavior is crucial in the design phase to avoid fatigue issues.



Figure 16 : Bluecopter® in flight.

Results of high-fidelity CFD/CSM-coupled simulations of the complete Bluecopter® using FLOWer/CAMRAD-II codes as well as unsteady pressure data on the T-Tail measured in flight were available for comparison^[25]. The selected flight case was level flight at 130kt.

For the sake of comparison, the exact same set of near-body and background meshes from the FLOWer/CII simulations were used in the elsA with PBM computations. However, the components connecting the rotor hub to the blades, such as the horns and necks were not present in the model, since in the PBM approach the blades are replaced by an actuator disk. The actuator disk mesh required a fine azimuthal discretization (1080 points) to allow for a proper representation of the blade planform which included a double sweep near the blade tip (Figure 17). The grid was deformed to account for coning and flapping angles, resulting in a displacement of the blade tip position compared to a flat disk of up to 30cm (rear blade).

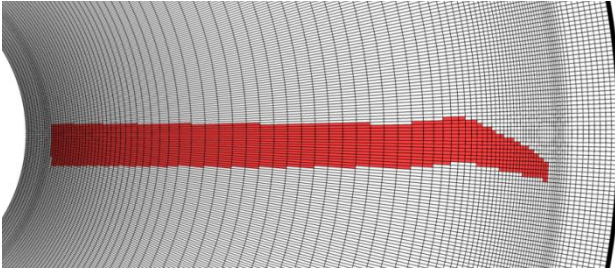


Figure 17: Blade planform representation through the activation of source terms in the disk mesh.

In addition to main rotor and Fenestron® actuator disk meshes, the assembly also includes (Figure 18):

- Two Cartesian background grids. The inner, finer mesh allows transferring the information between the near-body meshes and the outer background grid
- Near-body meshes of the cabin, landing skids, rear parts, Fenestron®, chimney and rotor head.

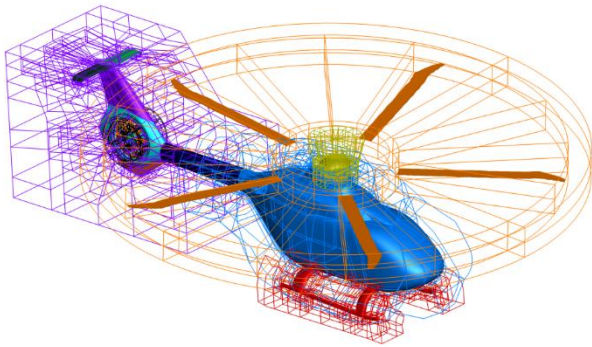


Figure 18: Mesh assembly components.

The different components are assembled using the Chimera technique (Figure 19). The complete mesh counts 79.1M elements distributed over 1800 blocks.

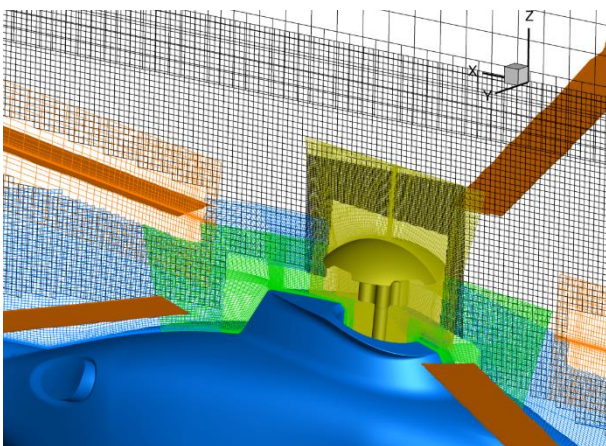


Figure 19: Detailed view of the mesh assembly near the rotor head.

In order to reduce the complexity of the numerical setup, all mesh components are static in the PBM simulations, including the main rotor head and the Fenestron® hub. As for the previous application cases, masking and interpolation coefficient determination operations are performed once in the beginning of the simulation.

Main rotor and Fenestron® aerodynamic loads, inputs for the PBM, were obtained from the FLOWer/CII simulations as no HOST model of this aircraft was available. Nevertheless, this allows for a direct comparison of the PBM approach to the complete H/C model. Indeed, the choice of the induced velocity model in HOST may considerably change the resulting rotor loads. Radial loads distributions were extracted over one rotor revolution for the main rotor and averaged over 5 revolutions for the Fenestron® due to the fact the blades are not evenly distributed (Figure 20).

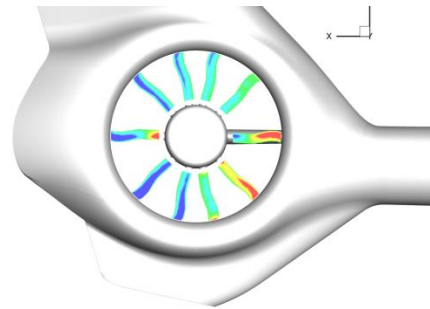


Figure 20: Example of Y Momentum source terms on Fenestron® blades with PBM approach.

Solution is obtained after 5 rotor revolutions at a time step equivalent to $\Delta\Psi = 10^\circ$, then 2 rotor revolutions at $\Delta\Psi = 1^\circ$ and 20 sub-iterations in both cases. To perform those convergence steps, it took around 3 times less than a complete H/C FLOWer/CII simulation.

The resulting dynamic loads integrated over each side of the horizontal stabilizer are presented in Figure 21. Only vertical force and pitching moment are shown as they are dominant on a horizontal stabilizer compared to the other components. They are normalized by the average total load obtained in the FLOWer/CII simulation. The curves show a good agreement between both numerical approaches in terms of amplitudes, even though an offset of about 20% in the average value is observed. Nevertheless, the dynamics (peak-to-peak) is well captured by the PBM, which is particularly useful for fatigue analysis.

Figure 22 and Figure 23 present Q-criterion iso-surfaces from PBM and FLOWer/CII simulations. Overall, the unsteady structures generated by the rotor are rather similar. One can observe in particular the vertical position of the blade tip vortices compared

to the horizontal stabilizer of the T-Tail are comparable and that this distance is of a few centimeters. It highlights the importance of accounting for rotor coning and flapping angles in the

actuator disk mesh, so the blade tip vortices are generated in the correct position.

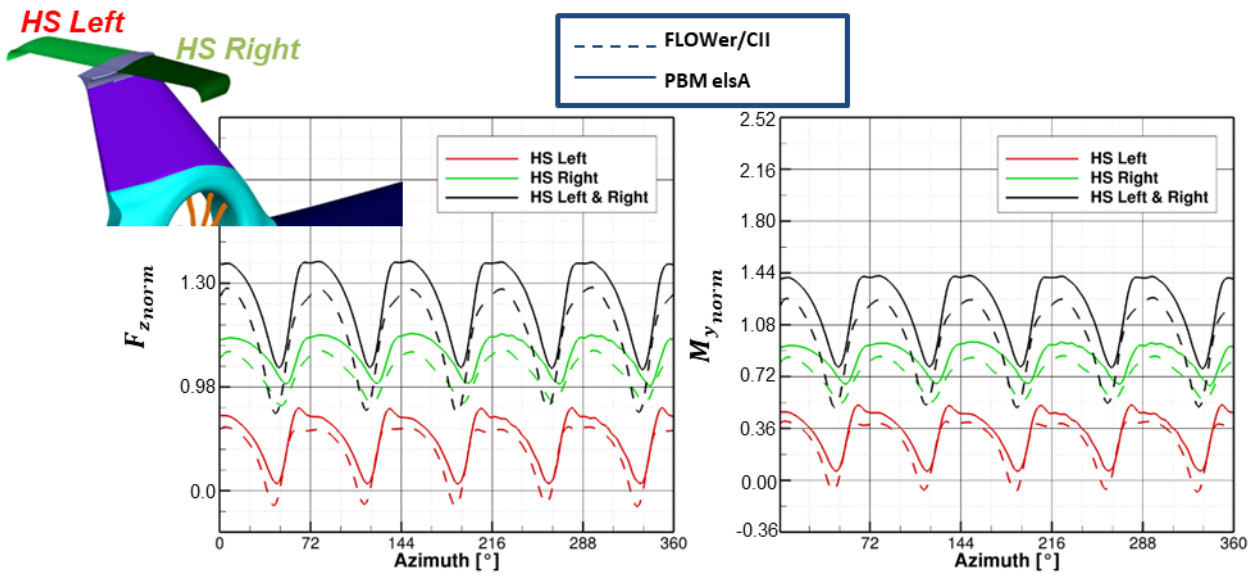


Figure 21: Dynamic loads on the horizontal stabilizer over one rotor revolution. Normalized vertical force and pitching moment. Comparison between numerical simulations with PBM (solid lines) and FLOWer/CII complete H/C^[25] (dashed lines).

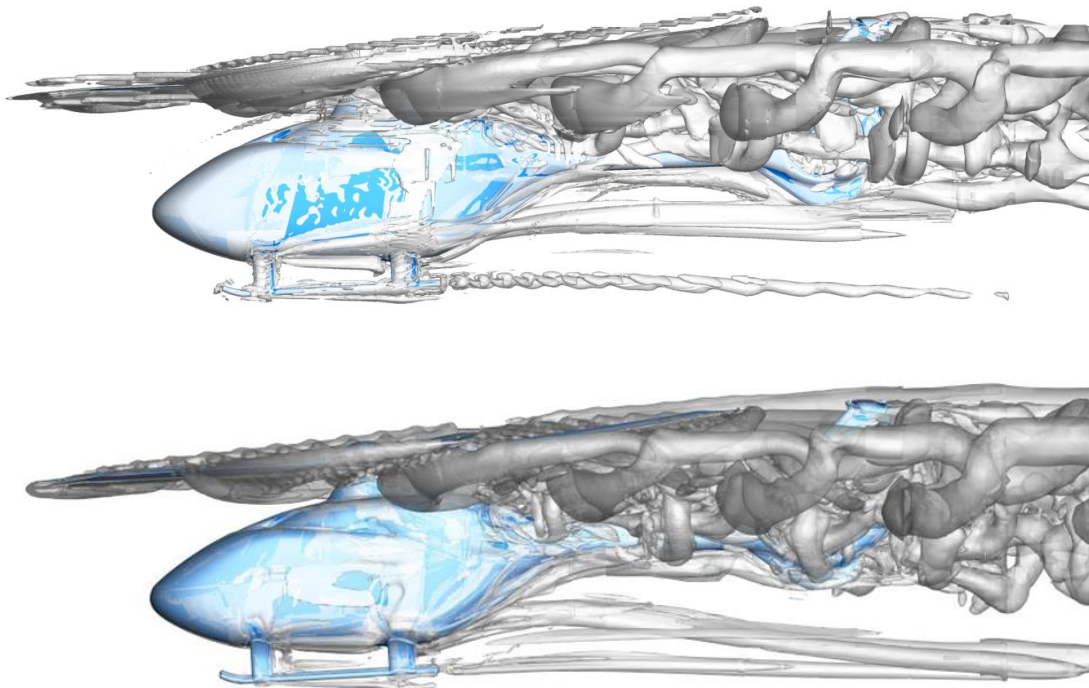


Figure 22: Flow visualization of rotor unsteady structures through Q-criterion iso-surfaces. Comparison between numerical simulations with PBM (top) and FLOWer/CII complete H/C^[25] (bottom). Left view.

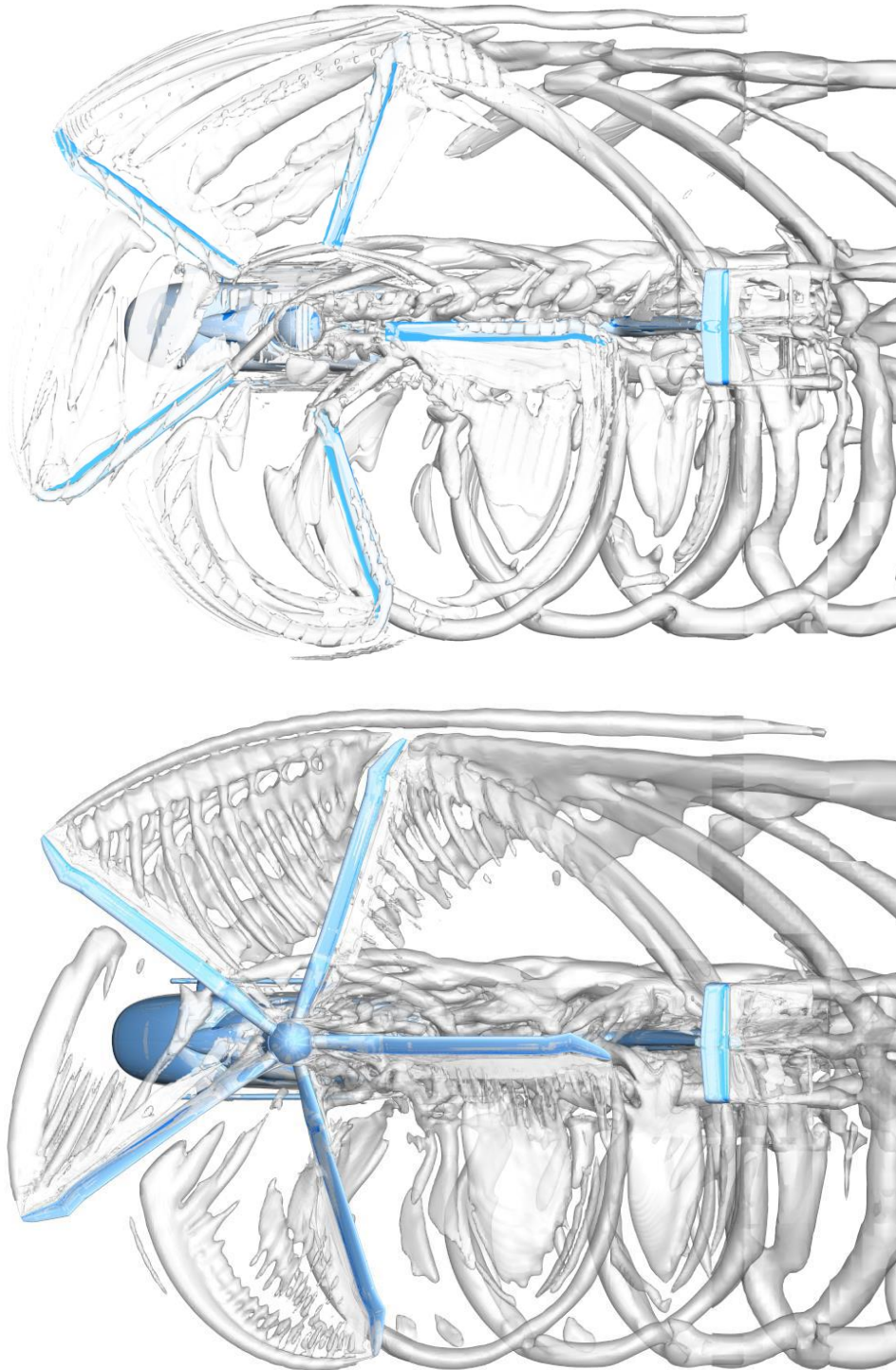


Figure 23: Flow visualization of rotor unsteady structures through Q-criterion iso-surfaces. Comparison between numerical simulations with PBM (top) and FLOWer/CII complete H/C^[25] (bottom). Top view.

Regarding flight tests, post-processed unsteady pressure data of six probes on the upper and lower surfaces of the horizontal stabilizer was available.^[25] It allows for checking the ability of the PBM to capture the local pressure average and dynamics due to interactions with the rotor wake.

Figure 24 compares the C_p evolution on 6 probes locations on the surface of the horizontal stabilizer of the T-Tail between numerical approaches (PBM, FLOWer/CII) and phase-averaged flight test data. Deltas between lower and upper surfaces C_p levels near the stabilizer tips are also shown (L1-U1, L4-

U2). Note that in this case the pressure coefficient is normalized by the upstream dynamic pressure, i.e:

$$(6) \quad C_p = \frac{p - p_{inf}}{0.5 \rho V_{inf}^2}$$

In general, the PBM almost consistently reproduced the results of FLOWer/CII. Indeed, peak-to-peak levels and phase resulting from PBM computations are nearly identical to FLOWer/CII results. With the exception of locations L1 and L3, the average value is also consistent between both numerical approaches. However, in positions L1 and L3, lower average C_p levels with the PBM are observed which could be due to missing rotor head elements. Nevertheless, these results are in line with the higher

integrated loads obtained with PBM compared to FLOWer/CII, as presented in Figure 21.

Compared to flight test measured data, both numerical methods systematically overestimated the average C_p , although the dynamics, including amplitudes and slopes, were quite well captured. Rinker & al.^[25] have explained that the presence of fairing plates around the pressure probes installed on the T-Tail surfaces have a significant impact on the average pressure and have shown that a CFD-based correction yields a much better correlation between FLOWer/CII and flight tests results. The corrected flight test data is not presented in this paper as the pressure correction offsets were not available.

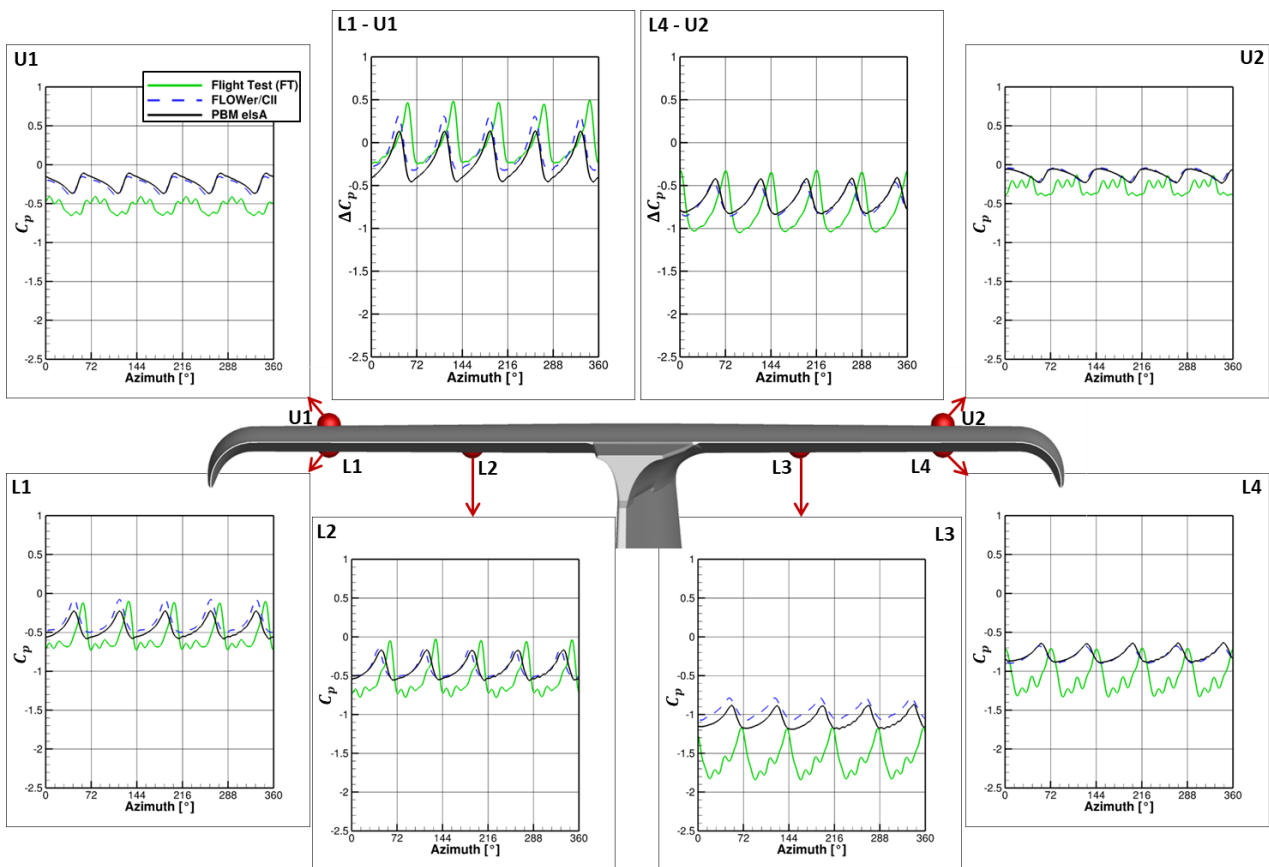


Figure 24: Comparison of C_p evolution on 6 probes locations on the surface of the horizontal stabilizer of the T-Tail between numerical approaches (PBM, FLOWer/CII) and phase-averaged flight test data from Rinker et al.^[25]. Deltas between lower and upper surfaces C_p levels near the stabilizer tips are also shown. Rear view of the T-Tail.

4. CONCLUSION

This paper has presented the implementation of the Phantom Blade Model, an unsteady actuator disk-like approach for modeling the rotor wake. It is based on the body-force and external coupling capabilities in elsA CFD code.

PBM results were confronted to higher-fidelity CFD models and to available experimental data in three

application cases. First, comparisons of blade tip vortices trajectories of an isolated two-bladed rotor in hover between measured data, CFD simulations with meshed blades and with PBM showed a quite good agreement with both tests and computations, but with half the CPU time. PBM results were improved when using rotor loads from meshed-blades simulations compared to HOST loads. Second, wind tunnel test unsteady pressure data of the ROBIN equipped with

a four-bladed rotor was compared to CFD simulations with PBM and with meshed blades. Both meshed-blades and PBM simulations revealed a shift in phase and in average pressure for some of the probes. Nevertheless, the PBM was able to capture interactions similar to a simulation with meshed-blades, but with 63% less CPU time. Actuator disk grid refinement to reduce numerical dissipation would be recommended. Finally, both main rotor and Fenestron® of the Bluecopter® were modelled using PBM. Dynamic behavior of total loads on the T-Tail horizontal surface were comparable between FLOWer/CII CFD/CSM-coupled simulations and PBM, even though an average offset was observed. Unsteady local pressure dynamic characteristics were well captured by both numerical methods, but overestimated the average level compared to flight test measurements.

In conclusion, the PBM approach showed promising results in the prediction of rotor and fixed parts dynamic interactions with a significant reduction in pre-processing and computational time. It could allow, for example, accounting for dynamic interactions criteria in the design of rear parts earlier in the development and/or in optimization loops. As a perspective for improving the methodology, it would be of interest to couple the CFD code to HOST to replace the induced velocity model by the CFD velocity field, resulting in more representative rotor loads distribution.

5. ACKNOWLEDGEMENTS

This work was supported by the CHALLENGE AeRothermoMEchanique (CHARME) Research Project, partially funded by the Direction Générale de l'Armement (DGA) and Direction Générale de l'Aviation Civile (DGAC).

6. NOMENCLATURE

c	Local chord	[m]
C_p	Pressure coefficient	[-]
C_T	Rotor thrust coefficient	[-]
dr	Blade element length	[m]
i	Coordinates index - x, y, z	[-]
F_i	Rotor aerodynamic loads - $i = x, y, z$	[N]
F_{znorm}	Normalized vertical force	[-]
Ma	Mach number	[-]
M_{ynorm}	Normalized pitching moment	[-]
μ	Rotor advance ratio	[-]
Ω	Rotor rotating speed	[rpm]
p	Pressure	[Pa]
p_{inf}, p_0	Upstream pressure	[Pa]

Ψ	Blade azimuthal position	[°]
$\Delta\Psi$	Rotation angle between time steps	[°]
ρ_{inf}	Upstream density	[kg/m ³]
S_i	Momentum source terms - $i = x, y, z$	[N/m ³]
S_E	Energy source term	[N/m ² s]
S	Source term	[N/m ³]
t	Current time	[s]
θ	Blade pitch angle	[°]
\bar{x}	Normalized chordwise coordinate (x/c)	[-]
(x', y')	Coordinates of blade local frame	[m]
Vol	Cell volume	[m ³]
v_i	Local velocities - $i = x, y, z$	[m/s]
V_{inf}	Upstream velocity	[m/s]
V_{tip}	Blade tip velocity	[m/s]

7. ABBREVIATIONS

CAMRAD-II or CII	Comprehensive Analytical Model of Rotorcraft Aerodynamics and Dynamics
CFD	Computational Fluid Dynamics
CHARME	CHALLENGE AeRothermoMEchanique
CSM	Computational Structural Mechanics
DTS	Dual-Time Step
elsA	Ensemble Logiciel de Simulation Aérodynamique
HOST	Helicopter Overall Simulation Tool
H/C	Helicopter
PBM	Phantom Blade Model
URANS	Unsteady Reynolds-Averaged Navier-Stokes
ROBIN	ROtor-Body INteraction
SST	Shear Stress Transport

8. REFERENCES

- [1] Altmikus, A. Wagner, S., Beaumier, P., Servera, G., "A Comparison: Weak versus Strong Modular Coupling for Trimmed Aeroelastic Rotor Simulations", American Helicopter Society 58th Annual Forum, June 2002
- [2] Dietz, M., Krämer, E., Wagner, S. and Altmikus, A., "Weak Coupling for Active Advanced Rotors. Analysis of a 2/rev Control Law for Power Reduction on a Trimmed Servo Flap Rotor using CFD." 31st European Rotorcraft Forum, Florence, Italy, September 2005

- [3] L. Cambier, S. Heib and S. Plot, "The ONERA elsA CFD Software: Input From Research and Feedback From Industry", *Mechanics & Industry*, Vol. 14, No. 3, pp. 159-174, 2013
- [4] Tadghighi, H., "Simulation of Rotor-Body Interactional Aerodynamics: An Unsteady Rotor Source Distributed Disk Model," *Proceedings of the 57th Annual Forum, American Helicopter Soc., Paper 57-00145*, Washington, D.C., 2001
- [5] Taewoo Kim, Sejong Oh, and Kwanjung Yee, "Novel Actuator Surface Method for Helicopter Rotor Analysis", *Journal of Aircraft*, Vol. 53, No. 6, pp. 1947-1952, 2016
- [6] Le Chuiton, F., "Actuator disc modelling for helicopter rotors". *Aerospace Science and Technology* 8, pp. 285–297, 2004
- [7] Thollet, W., Dufour, G., Carbonneau, X. and Blanc, F., "Body-force modeling for aerodynamic analysis of air intake – fan interactions", *International Journal of Numerical Methods for Heat & Fluid Flow*, Vol. 26 No. 7, pp. 2048-2065, 2016
- [8] Benoit, B., Dequin, A.M. & Kampa, K., VonGrünhagen W., Basset P.M. & Gimonet, B., "HOST, a general helicopter simulation tool for Germany and France", *56th Annual Forum of the American Helicopter Society*, 2000
- [9] L. Cambier, M. Gazaix, S. Heib, S. Plot, M. Poinot, et al., "An Overview of the Multi-Purpose elsA Flow Solver", *AerospaceLab*, p. 1-15, 2011
- [10] F. R. Menter, "Improved Two Equation k- ω Turbulence Models for Aerodynamic Flows", *Technical Report NASA Technical Memorandum 103975*, 1992
- [11] F. R. Menter, "Zonal Two Equation k- ω Turbulence Models for Aerodynamic Flows", *AIAA paper 93-2906 Proceedings of the 24th Fluid Dynamics Conference*, 1993
- [12] Jameson, A., Schmidt, W., Turkel, E., "Numerical solution of the Euler equations by finite volume methods using Runge Kutta time stepping schemes." *AIAA Paper 1981-1259, Proc. 14th Fluid and Plasma Dynamics Conference*, Palo Alto, California, USA, 1981
- [13] Steger, J., Dougherty, F., Benek, J., "A Chimera Grid Scheme.", *ASME Mini-symposium on advances in grid generation*, Houston, USA, 1993
- [14] Benoit, C., Jeanfaivre, G., Canonne, E., "Synthesis of ONERA Chimera method developed in the frame of CHANCE program.", *31st European Rotorcraft Forum*, Florence, Italy, 2005
- [15] Melson, N., Sanetrik, M., "Multigrid Acceleration of Time-Accurate Navier-Stokes Calculations.", *7th Copper Mountain Conference on Multigrid Methods*, Copper Mountain (CO), USA, 1995
- [16] Caradonna F. X. and Tung C., "Experimental and Analytical Studies of a Model Helicopter Rotor in Hover", *NASA TM 81232*, 09/1981
- [17] C. E. Freeman and R. E. Mineck, "Fuselage Surface Pressure Measurements of a Helicopter Wind Tunnel Model with a 3.15 meter Diameter Single Rotor", *NASA TM 80051*, March 1979
- [18] Markus Dietz, Thomas Kneisch, German Roth, A. D'Alascio and Dieter Schimke "EC145 T2: Comprehensive and Challenging Industrial CFD Applications", *American Helicopter Society 68th Annual Forum*, Fort Worth, Texas, May 1-3, 2012
- [19] A. Dehondt, F. Toulmay, "Influence of fuselage on rotor inflow performance and trim", *Vertica* vol. 14-4, pp 573 – 585, 1990
- [20] Hamers, M., Basset, P-M., "Application of the Finite State Unsteady Wake Model in Helicopter Flight Dynamic Simulation", *26th ERF conference*, La Hague, September 2000
- [21] Jeong, J., & Hussain, F. "On the identification of a vortex", *Journal of Fluid Mechanics*, 285, 69-94, 1995
- [22] A. R. Kenyon and R. E. Brown, "Wake Dynamics and Rotor-Fuselage Aerodynamic Interactions", *Journal of the AHS* vol. 54, 2009
- [23] B. S. Lee, M. S. Jung, O. J. Kwon and H. J. Kang, "Numerical Simulation of Rotor-Fuselage Aerodynamic Interaction Using an Unstructured Overset Mesh Technique", *J of Aeronautical & Space Sciences* Vol. 11, March 2010
- [24] Bebesel, M., D'Alascio, A., Schneider, S., Guenther, S., Vogel, F., Wehle, C., and Schimke, D., "Bluecopter demonstrator – an approach to eco-efficient helicopter design," *41st European Rotorcraft Forum*, Munich, Germany, 2015
- [25] Rinker, M., Ries, T., Embacher, M., Platzer, S., Uhl, G., Hajek, M., "Simulation of Rotor–Empennage Interactional Aerodynamics in Comparison to Experimental Data", *Vertical Flight Society 75th Annual Forum & Technology Display*, Philadelphia, Pennsylvania, USA, May 13–16, 2019

Copyright Statement

The authors confirm that they, and/or their company or organization, hold copyright on all of the original material included in this paper. The authors also confirm that they have obtained permission, from the copyright holder of any third party material included in this paper, to publish it as part of their paper. The authors confirm that they give permission, or have obtained permission from the copyright holder of this paper, for the publication and distribution of this paper as part of the ERF proceedings or as individual offprints from the proceedings and for inclusion in a freely accessible web-based repository.